
Scalable Visual State Space Model with Fractal Scanning

Lv Tang, HaoKe Xiao, Peng-Tao Jiang, Hao Zhang, Jinwei Chen, Bo Li
vivo Mobile Communication Co., Ltd
{lvtang, xiaohaoke, pt.jiang, haozhang, jinwei.chen, libra}@vivo.com

Abstract

Foundational models have significantly advanced in natural language processing (NLP) and computer vision (CV), with the Transformer architecture becoming a standard backbone. However, the Transformer’s quadratic complexity poses challenges for handling longer sequences and higher resolution images. To address this challenge, State Space Models (SSMs) like Mamba have emerged as efficient alternatives, initially matching Transformer performance in NLP tasks and later surpassing Vision Transformers (ViTs) in various CV tasks. To improve the performance of SSMs, one crucial aspect is effective serialization of image patches. Existing methods, relying on linear scanning curves, often fail to capture complex spatial relationships and produce repetitive patterns, leading to biases. To address these limitations, we propose using fractal scanning curves for patch serialization. Fractal curves maintain high spatial proximity and adapt to different image resolutions, avoiding redundancy and enhancing SSMs’ ability to model complex patterns accurately. We validate our method in image classification, detection, and segmentation tasks, and the superior performance validates its effectiveness.

1 Introduction

Foundational models have rapidly evolved within the domains of natural language processing (NLP) and computer vision (CV), giving rise to a plethora of works [4, 28, 17, 2, 25, 34, 26, 14], such as LLaVA [19] and BLIP-2 [16]. The common backbone of modern foundational models is Transformer [35], a type of sequence model. Although the self-attention mechanism in Transformer ensures effective modeling of complex data across varied contexts, its quadratic complexity poses significant efficiency challenges, thus presenting challenges to the further advancement of foundational models when facing longer language lengths or larger image resolutions.

Recently, based on State Space Model (SSM), Mamba [7] initially achieves performance comparable to that of Transformer in NLP with linear time complexity. Subsequently, researchers have made further improvements to Mamba [13, 38, 41, 20], enabling it to surpass the Visual Transformer (ViT) in different CV tasks, such as image classification and semantic segmentation. These developments have inspired further exploration into SSMs to ascertain their potential as viable alternatives to ViTs.

For fully leveraging the modeling capabilities of SSMs in CV tasks, one of the primary challenges is the effective serialization of image patches. Effective serialization can accurately represent and retain the intricate spatial relationships and structural properties inherent in images as far as possible, which are essential for SSMs to capture the representation of images. Consequently, numerous studies have designed various scanning mechanisms to optimize the serialization. For example, ViM [41] employs a bi-directional scanning curve that processes image patches horizontally (row by row) to capture spatial dependencies. Building upon this, VMamba [20] adds serialization along vertical

This paper is working in progress.

columns (column by column), enriching the analysis of spatial relationships. LocalMamba [13] introduces a window mechanism that divides the image into windows, serializing image patches within each window first, and then similarly processing between windows, which helps SSMs in capturing comprehensive image features.

Although the above methods have achieved notable performance, they generally utilize linear scanning curves, such as Zigzag, which may have inherent limitations and fail to fully capture the complex spatial relationships and structural properties within images. Additionally, these linear scans tend to produce repetitive scanning cycles, leading to serialized sequences that fall into repetitive patterns. This redundancy can introduce biases in the subsequent modeling by SSMs, as the model might overfit to these repetitive patterns rather than capturing the true underlying dynamics of the image. For example, the reliance on fixed scanning patterns may limit the model’s ability to adapt to dynamic changes in image resolution, further constraining its applicability across various imaging conditions.

To address these deficiencies, inspired by fractal theories [6], we propose employing fractal scanning curves as a more advanced method for patch serialization. Unlike linear curves, fractal curves preserve spatial proximity during the serialization process and adapt seamlessly to varying image resolutions. This adaptability ensures the preservation of the curve’s properties across different image dimensions, enabling a consistent approach to patch serialization that circumvents the limitations of repetitive scanning cycles typical of linear curves. This improved modeling capability enables SSMs to produce more accurate and contextually relevant predictions, fully harnessing the state space approach to dynamically capture and analyze complex patterns in images.

However, the application of fractal scanning curves in SSMs for image processing has identified certain limitations, particularly regarding the imperfect preservation of local adjacency and occasional disruptions in local continuity. These issues may result in the partial loss of local proximity information, which is essential for precise modeling by SSMs. To overcome this challenge, we propose a simple yet effective adjustment to the fractal curves. We implement a shift operation, adjusting the curves vertically by one pixel. This minor alteration significantly enhances local adjacency and continuity during pixel serialization. By more closely aligning the curve with the inherent spatial relationships within the image, this adjustment effectively addresses gaps and overlaps at critical junctions and complex sections of the curve, where adjacency might otherwise be compromised. In conclusion, our study contributes several key advancements, outlined as follows:

- We identify and address the inherent limitations of linear scanning curves traditionally used in SSMs. By analyzing their inefficiencies, we advocate for the adoption of fractal scanning curves, which are better suited to preserving the continuity of images.
- We further refine the fractal scanning curve approach by implementing a shift operation. This modification enhances the curve’s ability to preserve local structures and relationships within the image, thus addressing issues of imperfect adjacency and continuity disruptions commonly associated with standard fractal curves.
- We rigorously evaluate the efficacy of our innovations across three computer vision tasks: classification, segmentation, and detection. The experimental results unequivocally demonstrate enhanced performance and broad applicability of our proposed methods.

2 Related Work

2.1 Vision Backbone Architecture

In the domain of vision backbone architectures, significant advancements have been achieved through the development and refinement of several key frameworks. The existing widely used backbones contain CNN-based and ViT-based, each offering unique advantages and suited for different tasks within the field of CV. CNNs [15, 30, 11, 12, 29] have been foundational in the progress of vision models, predominantly due to their ability to capture spatial hierarchies in images. Pioneering models like AlexNet [15], VGG [30], and ResNet [11] have set the benchmarks in various vision tasks and continue to be pivotal in many applications. ViTs [35, 5, 22, 33] represent a paradigm shift in vision processing by applying the principles of self-attention across patches of an image, treating them akin to tokens in natural language processing. This architecture not only capitalizes on the Transformer’s ability to handle long-range dependencies but also sets a robust foundation for the explosion of modern foundational models [4, 28, 17, 2, 25, 34, 26, 14, 19, 16]. However, despite their remarkable

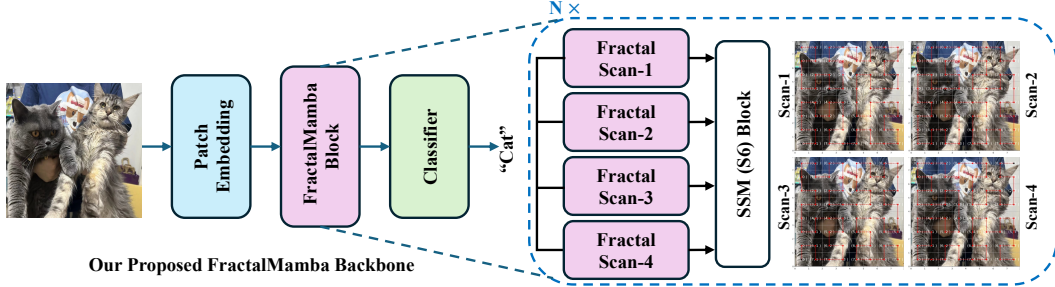


Figure 1: The architecture of our proposed FractalMamba Backbone. The FractalMamba block contains four curves in 4 directions. Taking 8×8 image patches for example, the first curve is from $(0,0)$ to $(7,0)$, the second curve is from $(0,0)$ to $(0,7)$, the third curve is from $(7,7)$ to $(7,0)$, and the fourth curve is from $(7,7)$ to $(0,7)$.

performance, ViTs face significant efficiency challenges due to their quadratic complexity, which poses obstacles to further advancements in foundational models, particularly when dealing with longer sequences or larger image resolutions.

More recently, SSMs have been proposed as an alternative backbone architecture for vision tasks [13, 38, 41, 20, 27], offering linear time complexity. SSMs employ a novel approach by modeling data sequences through state transitions, which is particularly advantageous for capturing dynamic changes in images. This emerging field seeks to provide more efficient solutions compared to traditional CNNs and Transformers. A critical issue in designing SSM-based visual backbones is how to effectively serialize image patches, transitioning from 2D to 1D while preserving the structural information in the image. This ensures that the SSM can accurately capture the current feature representation of the image. In this paper, we highlight the problems with current serialization methods and introduce a fractal serialization mechanism to enhance the performance of SSM-based backbones.

2.2 State Space Model

Drawing on principles from control theory, linear state space equations have been integrated with deep learning to enhance sequential data modeling, as demonstrated in works like HiPPO [8] and LSSL [10]. Recent advancements have enabled SSMs to increasingly compete with CNNs and Transformers in terms of performance. Notably, the Structured State Space Sequence Model (S4) [9] utilizes a linear state space for contextualization and has exhibited strong performance across various sequence modeling tasks, particularly with lengthy sequences. Subsequently, Mamba [7] has achieved a significant breakthrough with its linear-time inference and efficient training process, incorporating a selection mechanism and hardware-aware algorithms. Building on the success of Mamba, subsequent studies have explored the potential of SSMs for CV tasks [13, 38, 41, 20], achieving performance comparable to that of Transformers.

At the core of these endeavors is the development of various linear scanning mechanisms for serialization, as highlighted in recent surveys [37, 39]. However, linear scanning curves have inherent limitations and often fail to fully capture the complex spatial relationships within images. Furthermore, these linear scans can lead to repetitive scanning cycles, creating serialized sequences that exhibit redundant patterns. This redundancy can introduce biases in the subsequent modeling by SSMs, as the model may overfit to these repetitive patterns rather than capturing the true underlying dynamics of the image. To overcome these deficiencies, we propose the adoption of fractal scanning curves, which offer a more advanced approach to serialization. As shown in Fig. 1, following works [20, 13], we use the S6 block in the FractalMamba block. Moreover, the FractalMamba block contains four curves in 4 directions.

3 Method

3.1 Preliminaries

State Space Model. SSM provides a robust framework for modeling physical systems, particularly Linear Time-Invariant (LTI) systems. These models excel in representing such systems through a set

of first-order differential equations, effectively capturing the dynamics of the system’s state variables:

$$\begin{aligned} h'(t) &= \mathbf{A}h(t) + \mathbf{B}x(t), \\ y(t) &= \mathbf{C}h(t). \end{aligned} \quad (1)$$

$h'(t)$ denotes the time derivative of the state vector $h(t)$, with matrices \mathbf{A} , \mathbf{B} , \mathbf{C} defining the relationships between the $h(t)$, $x(t)$, $y(t)$. This system uses $\mathbf{A} \in \mathbb{R}^{N \times N}$ as the evolution parameter and $\mathbf{B} \in \mathbb{R}^{N \times 1}$, $\mathbf{C} \in \mathbb{R}^{1 \times N}$ as the projection parameters.

Since SSMs operate on continuous sequences $x(t)$, they are unable to process discrete token inputs such as images and texts. Consequently, the adaptation to a discretized version of the SSM becomes essential. As described in Mamba [7], the commonly used method for transformation \mathbf{A} , \mathbf{B} from continuous to discrete form is zero-order hold (ZOH), which is defined as follows:

$$\begin{aligned} \bar{\mathbf{A}} &= \exp(\Delta \mathbf{A}), \\ \bar{\mathbf{B}} &= (\Delta \mathbf{A})^{-1}(\exp(\Delta \mathbf{A}) - \mathbf{I}) \cdot \Delta \mathbf{B}. \end{aligned} \quad (2)$$

Δ is the timescale parameter to transform the continuous parameters \mathbf{A} , \mathbf{B} to discrete parameters $\bar{\mathbf{A}}$, $\bar{\mathbf{B}}$. After the operation, the discretized version of Eqn. 1 can be rewritten as:

$$\begin{aligned} h_t &= \bar{\mathbf{A}}h_{t-1} + \bar{\mathbf{B}}x_t, \\ y_t &= \mathbf{C}h_t. \end{aligned} \quad (3)$$

At last, the models compute output through a global convolution:

$$\begin{aligned} \bar{\mathbf{K}} &= (\mathbf{C}\bar{\mathbf{B}}, \mathbf{C}\bar{\mathbf{A}}\bar{\mathbf{B}}, \dots, \mathbf{C}\bar{\mathbf{A}}^{L-1}\bar{\mathbf{B}}) \\ \mathbf{y} &= \mathbf{x} * \bar{\mathbf{K}}, \end{aligned} \quad (4)$$

where L is the length of the input sequence \mathbf{x} , $\bar{\mathbf{K}} \in \mathbb{R}^L$ is a structured convolutional kernel and $*$ represents the convolution operation.

Selective SSMs. The inherent LTI characteristic of SSMs, characterized by the consistent application of matrices $\bar{\mathbf{A}}$, $\bar{\mathbf{B}}$, $\bar{\mathbf{C}}$, and Δ across various inputs, limits their ability to adaptively filter and interpret contextual nuances within diverse input sequences. To overcome this limitation, we introduce Selective SSM as the core operator in our FractalMamba model. In Selective SSMs, the matrices $\bar{\mathbf{B}}$, $\bar{\mathbf{C}}$, and Δ are rendered as dynamic, input-responsive elements, effectively transitioning the SSM into a time-variant model. This modification enables the model to adapt more effectively to different input contexts, significantly enhancing its capacity to capture pertinent temporal features and relationships, and thereby improving the accuracy and efficiency of the input sequence representation.

3.2 Limitations of Existing Scanning Mechanisms

From Eqn. 1, it becomes evident that selecting the most appropriate inputs for each time step in the SSM is crucial for effectively capturing and modeling the feature representation of the current image. To achieve this, the serialization process from 2D images to 1D sequences must meticulously capture the inherent structural information within the image. This requires preserving the structural coherence among image patches, ensuring that the serialized form maintains the essential spatial relationships present in the original image.

Existing linear scanning methods, such as the Z-order or Zigzag curve, exhibit significant limitations in preserving spatial relationships. While these methods maintain adjacency information between neighboring patches within the same row, they fail to effectively capture inter-row relationships. This oversight leads to the loss of crucial structural links essential for understanding broader spatial relationships within the image. Consequently, such scanning techniques compromise the structural integrity of the original image, undermining the model’s capacity to accurately reflect the image’s true characteristics. This lack of structural fidelity results in a model that is insensitive to variations in image scale, meaning that correlations evident at lower resolutions may not be preserved at higher resolutions. As a result, patterns and features learned at a lower resolution often do not translate effectively to higher resolutions, limiting the model’s applicability across different scales.

To overcome these challenges, we introduce fractal scanning mechanisms in our model. These mechanisms are designed to more adeptly follow the complex contours and structures within an image, thereby preserving its integral structural characteristics across different viewing scales. In this paper, we choose the Hilbert curve, which is a typical fractal curve.

Algorithm 1 Hilbert Curve Generation

```
1: function HILBERT( $x_0, y_0, \vec{x}, \vec{y}, depth$ )
2:   if  $depth = 0$  then
3:     plot( $x_0 + (\vec{x}[0] + \vec{y}[0])/2, y_0 + (\vec{x}[1] + \vec{y}[1])/2$ )
4:   else
5:     HILBERT( $x_0, y_0, \vec{y}/2, \vec{x}/2, depth - 1$ )
6:     HILBERT( $x_0 + \vec{x}[0]/2, y_0 + \vec{x}[1]/2, \vec{x}/2, \vec{y}/2, depth - 1$ )
7:     HILBERT( $x_0 + \vec{x}[0]/2 + \vec{y}[0]/2, y_0 + \vec{x}[1]/2 + \vec{y}[1]/2, \vec{x}/2, \vec{y}/2, depth - 1$ )
8:     HILBERT( $x_0 + \vec{x}[0]/2 + \vec{y}[0], y_0 + \vec{x}[1]/2 + \vec{y}[1], \vec{y}/2, \vec{x}/2, depth - 1$ )
9:   end if
10: end function
```

3.3 Fractal Scanning Mechanisms

The Hilbert curve, a fractal defined through a recursive process, is particularly effective in image analysis because it maintains spatial and structural consistency at varying scales. Its property of self-similarity is vital for the analysis of high-resolution images, enabling it to capture features coherently across different scales. Starting from a single point, the Hilbert curve uses the midpoints of directional vectors \vec{x} and \vec{y} to dictate its path within the two-dimensional space. Through successive recursive subdivisions and traversals, the curve systematically accesses every part of the image, ensuring local continuity. This method effectively preserves the spatial relationships within the image, which is essential for delivering precise analysis and representation.

The Hilbert curve’s recursive design is inherently adaptable, allowing it to seamlessly conform to varying image resolutions. In this process, the vectors \vec{x} and \vec{y} are halved and swapped with each recursion, depending on the quadrant, illustrating the curve’s ability to efficiently and uniformly occupy two-dimensional spaces. This structured traversal technique ensures that image patches adjacent on the curve also remain adjacent in the image. Preserving this adjacency is key to maintaining the spatial relationships within the image.

As shown in Algorithm. 1, the use of vectors \vec{x} and \vec{y} in the pseudocode simplifies the understanding of directional movements and subdivisions within each recursive call, aligning the spatial mapping of the curve with the underlying pixel grid of the image. This alignment is pivotal in reducing the loss of important image features during the serialization processing, where maintaining the hierarchical structure of pixel data is paramount.

Curves Shifting. However, the use of fractal scanning curves in SSMs for image processing has revealed certain limitations, specifically concerning the imperfect maintenance of local adjacency and occasional disruptions in local continuity. As shown in Fig. 2, the two patches in the image, (3,3) and (3,4), are neighboring in terms of spatial location, but the distance between the two of them is not neighboring in the Hilbert scan. These issues can lead to a partial loss of local proximity information, which is crucial for accurate modeling by SSMs. To address this challenge, we introduce a simple yet effective modification to the fractal curves. We apply a shift operation, moving the curves up or down by one pixel. This minor modification significantly improves the local adjacency and continuity of pixel serialization. By aligning the curve more closely with the inherent spatial relationships within the image, this shift helps to mitigate gaps and overlaps at critical junctions and complex parts of the curve, where adjacency might originally be lost.

4 Experiments

In this section, we conduct a series of experiments to evaluate and compare FractalMamba with established benchmark models, including architectures based on CNNs and ViTs. Our assessment covers a range of visual tasks, such as image classification, object detection, and semantic segmentation. Following these evaluations, we provide a comprehensive analysis of FractalMamba’s characteristics,



Shifting Operation

Figure 2: The Hilbert curve and the corresponding shifting operation.

Table 1: Performance comparison of our FractalMamba and other methods on ImageNet-1K.

Models	Image Size	#Param.	FLOPs	ImageNet Top-1 Acc.
RegNetY-8G [29]	224 ²	39M	8.0G	81.7
EffNet-B5 [31]	456 ²	30M	9.9G	83.6
ViT-B/16 [5]	384 ²	86M	55.4G	77.9
DeiT-B [32]	224 ²	86M	17.5G	81.8
ConvNeXt-T [23]	224 ²	29M	4.5G	82.1
HiViT-S [40]	224 ²	38M	9.1G	83.5
Swin-T [22]	224 ²	28M	4.6G	81.3
ViM-S [41]	224 ²	26M	-	80.5
VMamba-T [20]	224 ²	31M	4.9G	82.5
LocalMamba-T [13]	224 ²	26M	5.7G	82.7
PlainMamba-L3 [38]	224 ²	50M	14.4G	82.3
FractalMamba-T	224 ²	31M	4.9G	82.7

with a particular emphasis on its standout feature: the remarkable capability to efficiently handle increasingly large input resolutions. Note that, in the following image classification, object detection, and semantic segmentation evaluation, we do not add the shifting operation, since it would introduce extra curves in different directions. For fair comparison with other works like VMamba, we only use four fractal curves. All experiment are conducted using 8 NVIDIA H800 GPUs.

4.1 Image Classification

Experiment Setting. We evaluate the performance of FractalMamba using the ImageNet-1K dataset [3], following the evaluation protocol described in the work [21]. The FractalMamba-T model is trained from scratch over 300 epochs, with an initial 20-epoch warm-up period, using a batch size of 1024. The training processes utilizes the AdamW optimizer [24], with betas set to (0.9,0.999), momentum of 0.9, a cosine decay learning rate scheduler, an initial learning rate of 1×10^{-3} , and a weight decay of 0.05. Additional strategies such as label smoothing (0.1) and exponential moving average (EMA) were incorporated into the training regimen. No other training techniques were used beyond these specified methods.

Model Performance. The comparison results of FractalMamba against benchmark backbone models on the ImageNet-1K dataset are summarized in Table. 1. Notably, with comparable FLOPs, FractalMamba-T achieves a performance of 82.5%, outperforming RegNetY-8G [29] by 0.8%, DeiT-S [32] by 0.7%, and Swin-T by 1.2%. Moreover, FractalMamba demonstrates competitive performance relative to other SSM-based models. One primary reason is that for images with low and fixed resolutions, linear scanning suffices for the model to learn the corresponding patterns, and thus the fractal scanning mechanism does not exhibit a distinct performance advantage. However, as detailed in Section 4.4, fractal curves, due to their unique self-similarity, effectively capture the structural information of images across varying resolutions, thereby exhibiting superior performance.

4.2 Object Detection

Experiment Setting. In this section, we evaluate the performance of FractalMamba on object detection using the MSCOCO 2017 dataset [18]. We configure our training setup using the MMDetection library [1], adhering to the hyper-parameters utilized in the Swin [22] model with the Mask-RCNN detector. Specifically, we use the AdamW optimizer [24] and fine-tune the pre-trained classification models (originally trained on ImageNet-1K) over both 12 and 36 epochs. For FractalMamba-T, the drop path rate is set at 0.2%. The learning rate starts at 1×10^{-4} and is reduced by a factor of 10 at the 9th and 11th epochs. Multi-scale training and random flipping are implemented with a batch size of 16, aligning with established best practices for object detection evaluations.

Model Performance. The results on the COCO dataset are summarized in Table 2. FractalMamba consistently outperforms other models in both box and mask AP, regardless of the training schedule employed. Specifically, with a 12-epoch fine-tuning schedule, FractalMamba-T models achieve object detection mean Average Precision (mAP) of 47.8%, which is superior to Swin-T by 5.1% mAP,

Table 2: The results of object detection and instance segmentation on the COCO dataset. FLOPs are calculated for an input size of 1280×800 . The metrics AP^b and AP^m represent box AP and mask AP, respectively. The notation ‘1 ×’ indicates that models were fine-tuned for 12 epochs, while ‘3 × MS’ denotes the utilization of multi-scale training across 36 epochs.

Mask R-CNN 1 × schedule								
Backbone	AP^b	AP_{50}^b	AP_{75}^b	AP^m	AP_{50}^m	AP_{75}^m	#param.	FLOPs
Swin-T	42.7	65.2	46.8	39.3	62.2	42.2	48M	267G
ConvNeXt-T	44.2	66.6	48.3	40.1	63.3	42.8	48M	262G
ViT-Adapter-S	44.7	65.8	48.3	39.9	62.5	42.8	48M	403G
VMamba-T	47.4	69.5	52.0	42.7	66.3	46.0	50M	270G
LocalMamba-T	46.7	68.7	50.8	42.2	65.7	45.5	45M	291G
PlainMamba-L3	46.8	68.0	51.1	41.2	64.7	43.9	79M	696G
FractalMamba-T	47.8	70.0	52.4	42.9	66.6	46.3	50M	270G
Mask R-CNN 3 × MS schedule								
Backbone	AP^b	AP_{50}^b	AP_{75}^b	AP^m	AP_{50}^m	AP_{75}^m	#param.	FLOPs
Swin-T	46.0	68.1	50.3	41.6	65.1	44.9	48M	267G
ConvNeXt-T	46.2	67.9	50.8	41.7	65.0	44.9	48M	262G
ViT-Adapter-S	48.2	69.7	52.5	42.8	66.4	45.9	48M	403G
VMamba-T	48.9	70.6	53.6	43.7	67.7	46.8	50M	270G
LocalMamba-T	48.7	70.1	53.0	43.4	67.0	46.4	45M	291G
FractalMamba-T	49.5	71.3	54.0	44.1	68.5	47.4	50M	270G

Table 3: Results of semantic segmentation on ADE20K using UperNet [36]. FLOPs are calculated with input size of 512×2048 . ‘SS’ and ‘MS’ denote single-scale and multi-scale testing, respectively.

Models	Crop Size	mIoU(SS)	mIoU(MS)	#param.	FLOPs
ResNet-50	512^2	42.1	42.8	67M	953G
DeiT-S+MLN	512^2	43.8	45.1	58M	1217G
Swin-T	512^2	44.4	45.8	60M	945G
ConvNeXt-T	512^2	46.0	46.7	60M	939G
VMamba-T	512^2	48.3	48.6	62M	948G
LocalMamba-T	512^2	47.9	49.1	57M	970G
PlainMamba-L2	512^2	46.8	-	55M	285G
FractalMamba-T	512^2	48.9	49.8	62M	948G

ConvNeXt-T by 3.6% mAP and VMamba-T by 0.4%. In the same configuration, FractalMamba-T achieves instance segmentation mean Intersection over Union (mIoU) of 42.9%, surpassing Swin-T by 3.6% mIoU and ConvNeXt-T by 2.7% mIoU. These results highlight FractalMamba’s capability to deliver robust performance in downstream tasks requiring dense prediction.

4.3 Semantic Segmentation

Experiment Setting. Following Swin [22], we augment the pre-trained model with an UperHead [36]. We employ the AdamW optimizer [24], setting the learning rate to 6×10^{-5} . The fine-tuning process extends over 160,000 iterations with a batch size of 16. The standard input resolution is 512×512 , and we additionally provide experimental results using 640×640 inputs along with multi-scale (MS) testing to evaluate performance enhancements at varied resolutions.

Model Performance. The results of semantic segmentation on the ADE20K dataset are summarized in Table. 3. In line with findings from previous experiments, FractalMamba exhibits superior accuracy. Specifically, FractalMamba-T achieves a mean Intersection over Union (mIoU) of 48.9% with a resolution of 512×512 , and 49.8% mIoU with multiscale (MS) input. These results surpass those of all benchmarked methods, including ResNet [11], DeiT [32], Swin [22], and ConvNeXt [23], confirming FractalMamba’s effectiveness in semantic segmentation tasks.

Table 4: The effectiveness of our proposed shifting operation.

Models	224 ²	384 ²	512 ²	640 ²	768 ²	1024 ²
FractalMamba	82.7	82.4	81.2	80.2	77.9	69.6
FractalMamba+Shifting	82.9	82.7	81.6	80.5	78.3	70.4

Table 5: Comparison of generalizability to image inputs with different spatial resolutions.

Models	Image Size	#Param.	FLOPs	ImageNet Top-1 Acc.
ResNet-50	224 ²	26M	4.1G	76.4
	384 ²	26M	12.1G	76.5
	512 ²	26M	21.5G	73.4
	640 ²	26M	33.5G	69.7
	768 ²	26M	48.3G	65.3
	1024 ²	26M	85.9G	52.1
ConvNeXt	224 ²	29M	4.5G	82.0
	384 ²	29M	13.1G	81.0
	512 ²	29M	23.3G	78.0
	640 ²	29M	36.5G	74.3
	768 ²	29M	52.5G	69.5
	1024 ²	29M	93.3G	55.4
DeiT	224 ²	22M	4.6G	80.7
	384 ²	22M	15.5G	78.9
	512 ²	22M	31.8G	74.2
	640 ²	22M	58.2G	68.0
	768 ²	22M	98.7G	70.0
	1024 ²	22M	243.1G	46.9
Swin	224 ²	28M	4.5G	81.2
	384 ²	28M	14.5G	80.7
	512 ²	28M	26.6G	79.0
	640 ²	28M	45.0G	76.6
	768 ²	28M	70.7G	73.1
	1024 ²	28M	152.5G	61.9
HiViT	224 ²	19M	4.6G	81.9
	384 ²	19M	15.2G	81.5
	512 ²	19M	30.6G	79.3
	640 ²	19M	54.8G	76.0
	768 ²	19M	91.4G	71.4
	1024 ²	19M	218.9G	58.9
VMamba	224 ²	31M	4.9G	82.5
	384 ²	31M	14.3G	82.5
	512 ²	31M	25.4G	81.1
	640 ²	31M	39.6G	79.3
	768 ²	31M	57.1G	76.1
	1024 ²	31M	101.5G	62.3
FractalMamba	224 ²	31M	4.9G	82.5
	384 ²	31M	14.3G	82.4
	512 ²	31M	25.4G	81.2
	640 ²	31M	39.6G	80.2
	768 ²	31M	57.1G	77.9
	1024 ²	31M	101.5G	69.6

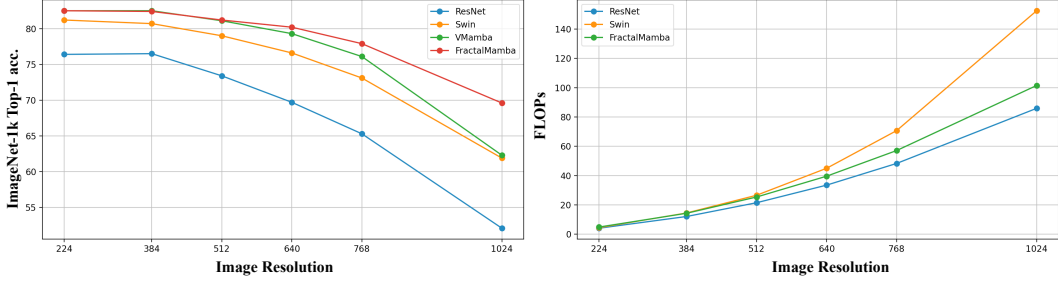


Figure 3: The variations in classification accuracy and computational complexity (FLOPs) as the resolutions of test images increase progressively.

4.4 Ablation Studies

The effectiveness of Shifting Operation. We identify an issue where the inherent structure of fractal curves could lead to a partial loss of local proximity information—an essential element for accurate modeling by SSMs. To overcome this limitation, we introduced a straightforward yet effective modification to the fractal curves by implementing a shift operation. This adjustment involves shifting the entire curve vertically or horizontally by one pixel. The effectiveness of this approach is quantitatively evaluated in Table. 4, where the adjusted fractal curves consistently outperform the traditional configurations in maintaining higher fidelity in feature representation.

Model Scalability and Efficiency. In this study, we conduct experiments to evaluate the scalability of FractalMamba and other SSM-based models with progressively larger input images. Specifically, models initially trained with an input size of 224×224 are applied directly to images with resolutions ranging from 384×384 to 1024×1024 . We assess their generalization performance by examining the number of parameters, FLOPs during both training and inference phases, and Top-1 classification accuracy on the ImageNet-1K dataset.

According to the results summarized in Table 3, FractalMamba exhibits the most consistent performance across varying input sizes, achieving a Top-1 classification accuracy of 69.6% with 101.5G FLOPs when the input resolution is increased to 1024×1024 . In comparison, Swin [22], with the same input size, achieves a Top-1 accuracy of 61.9% but experiences a significant drop to 19. In contrast, while ResNet50 [11] maintains a relatively high inference speed at the largest input resolution, its classification accuracy drops to 52.1%, underscoring its limited scalability. The performance changes across various resolutions for different models are intuitively depicted in Fig. 3. Notably, FractalMamba demonstrates a linear increase in computational complexity, as measured by FLOPs, closely mirroring the behavior of traditional CNN-based architectures. This observation substantiates the theoretical predictions regarding selective SSMs [7].

5 Conclusion

In this paper, we introduce a novel method for serializing image patches using fractal scanning curves to enhance the performance of SSMs in various computer vision tasks. Unlike traditional linear scanning curves, fractal curves exhibit superior handling of images across multiple scales by maintaining high spatial proximity and adapting seamlessly to different image resolutions. This approach not only reduces redundancy but also more accurately captures complex patterns within images. We validate our method across a range of computer vision tasks, including image classification, detection, and segmentation. The experimental results unequivocally demonstrate that fractal curve scanning significantly outperforms linear curve scanning in these applications. These findings underscore the practicality of fractal curves in vision tasks and pave the way for future research, such as exploring additional fractal scanning methods to further enhance model performance. We believe that with continued refinement, fractal curve usage in SSMs will become increasingly pivotal in future computer vision applications, particularly in processing high-resolution and large-scale image data. By advancing these models, our goal is to develop more efficient and accurate vision processing technologies to address the escalating demands of image data processing.

References

- [1] Kai Chen, Jiaqi Wang, Jiangmiao Pang, Yuhang Cao, Yu Xiong, Xiaoxiao Li, Shuyang Sun, Wansen Feng, Ziwei Liu, Jiarui Xu, et al. Mmdetection: Open mmlab detection toolbox and benchmark. *arXiv preprint arXiv:1906.07155*, 2019.
- [2] Aakanksha Chowdhery, Sharan Narang, Jacob Devlin, Maarten Bosma, Gaurav Mishra, Adam Roberts, Paul Barham, Hyung Won Chung, Charles Sutton, Sebastian Gehrmann, Parker Schuh, Kensen Shi, Sasha Tsvyashchenko, Joshua Maynez, Abhishek Rao, Parker Barnes, Yi Tay, Noam Shazeer, Vinodkumar Prabhakaran, Emily Reif, Nan Du, Ben Hutchinson, Reiner Pope, James Bradbury, Jacob Austin, Michael Isard, Guy Gur-Ari, Pengcheng Yin, Toju Duke, Anselm Levskaya, Sanjay Ghemawat, Sunipa Dev, Henryk Michalewski, Xavier Garcia, Vedant Misra, Kevin Robinson, Liam Fedus, Denny Zhou, Daphne Ippolito, David Luan, Hyeontaek Lim, Barret Zoph, Alexander Spiridonov, Ryan Sepassi, David Dohan, Shivani Agrawal, Mark Omernick, Andrew M. Dai, Thanumalayan Sankaranarayanan Pillai, Marie Pellat, Aitor Lewkowycz, Erica Moreira, Rewon Child, Oleksandr Polozov, Katherine Lee, Zongwei Zhou, Xuezhi Wang, Brennan Saeta, Mark Diaz, Orhan Firat, Michele Catasta, Jason Wei, Kathy Meier-Hellstern, Douglas Eck, Jeff Dean, Slav Petrov, and Noah Fiedel. Palm: Scaling language modeling with pathways. *J. Mach. Learn. Res.*, 24:240:1–240:113, 2023.
- [3] Jia Deng, Wei Dong, Richard Socher, Li-Jia Li, Kai Li, and Li Fei-Fei. Imagenet: A large-scale hierarchical image database. In *CVPR*, pages 248–255. IEEE, 2009.
- [4] Jacob Devlin, Ming-Wei Chang, Kenton Lee, and Kristina Toutanova. BERT: pre-training of deep bidirectional transformers for language understanding. In *NAACL*, pages 4171–4186, 2019.
- [5] Alexey Dosovitskiy, Lucas Beyer, Alexander Kolesnikov, Dirk Weissenborn, Xiaohua Zhai, Thomas Unterthiner, Mostafa Dehghani, Matthias Minderer, Georg Heigold, Sylvain Gelly, Jakob Uszkoreit, and Neil Houlsby. An image is worth 16x16 words: Transformers for image recognition at scale. In *ICLR*. OpenReview.net, 2021.
- [6] Craig Gotsman and Michael Lindenbaum. On the metric properties of discrete space-filling curves. *IEEE Trans. Image Process.*, 5(5):794–797, 1996.
- [7] Albert Gu and Tri Dao. Mamba: Linear-time sequence modeling with selective state spaces. *CoRR*, abs/2312.00752, 2023.
- [8] Albert Gu, Tri Dao, Stefano Ermon, Atri Rudra, and Christopher Ré. Hippo: Recurrent memory with optimal polynomial projections. In *NeurIPS*, 2020.
- [9] Albert Gu, Karan Goel, and Christopher Ré. Efficiently modeling long sequences with structured state spaces. In *ICLR*. OpenReview.net, 2022.
- [10] Albert Gu, Isys Johnson, Karan Goel, Khaled Saab, Tri Dao, Atri Rudra, and Christopher Ré. Combining recurrent, convolutional, and continuous-time models with linear state space layers. In *NeurIPS*, pages 572–585, 2021.
- [11] Kaiming He, Xiangyu Zhang, Shaoqing Ren, and Jian Sun. Deep residual learning for image recognition. In *CVPR*, pages 770–778. IEEE, 2016.
- [12] Andrew G. Howard, Menglong Zhu, Bo Chen, Dmitry Kalenichenko, Weijun Wang, Tobias Weyand, Marco Andreetto, and Hartwig Adam. Mobilenets: Efficient convolutional neural networks for mobile vision applications. *CoRR*, abs/1704.04861, 2017.
- [13] Tao Huang, Xiaohuan Pei, Shan You, Fei Wang, Chen Qian, and Chang Xu. Localmamba: Visual state space model with windowed selective scan. *CoRR*, abs/2403.09338, 2024.
- [14] Alexander Kirillov, Eric Mintun, Nikhila Ravi, Hanzi Mao, Chloe Rolland, Laura Gustafson, Tete Xiao, Spencer Whitehead, Alexander C. Berg, Wan-Yen Lo, Piotr Dollar, and Ross Girshick. Segment anything. In *ICCV*, pages 4015–4026, October 2023.
- [15] Alex Krizhevsky, Ilya Sutskever, and Geoffrey E. Hinton. Imagenet classification with deep convolutional neural networks. In *NIPS*, pages 1106–1114, 2012.
- [16] Junnan Li, Dongxu Li, Silvio Savarese, and Steven C. H. Hoi. BLIP-2: bootstrapping language-image pre-training with frozen image encoders and large language models. In *ICML*, volume 202, pages 19730–19742, 2023.
- [17] Junnan Li, Dongxu Li, Caiming Xiong, and Steven C. H. Hoi. BLIP: bootstrapping language-image pre-training for unified vision-language understanding and generation. In *ICML*, volume 162 of *Proceedings of Machine Learning Research*, pages 12888–12900. PMLR, 2022.
- [18] Tsung-Yi Lin, Michael Maire, Serge Belongie, James Hays, Pietro Perona, Deva Ramanan, Piotr Dollár, and C Lawrence Zitnick. Microsoft coco: Common objects in context. In *ECCV*, pages 740–755. Springer, 2014.
- [19] Haotian Liu, Chunyuan Li, Qingyang Wu, and Yong Jae Lee. Visual instruction tuning. *CoRR*, abs/2304.08485, 2023.
- [20] Yue Liu, Yunjie Tian, Yuzhong Zhao, Hongtian Yu, Lingxi Xie, Yaowei Wang, Qixiang Ye, and Yunfan Liu. Vmamba: Visual state space model. *CoRR*, abs/2401.10166, 2024.
- [21] Ze Liu, Han Hu, Yutong Lin, Zhuliang Yao, Zhenda Xie, Yixuan Wei, Jia Ning, Yue Cao, Zheng Zhang, Li Dong, et al. Swin transformer v2: Scaling up capacity and resolution. In *CVPR*, pages 12009–12019, 2022.

- [22] Ze Liu, Yutong Lin, Yue Cao, Han Hu, Yixuan Wei, Zheng Zhang, Stephen Lin, and Baining Guo. Swin transformer: Hierarchical vision transformer using shifted windows. In *ICCV*, pages 9992–10002. IEEE, 2021.
- [23] Zhuang Liu, Hanzi Mao, Chao-Yuan Wu, Christoph Feichtenhofer, Trevor Darrell, and Saining Xie. A convnet for the 2020s. In *CVPR*, pages 11966–11976. IEEE, 2022.
- [24] Ilya Loshchilov and Frank Hutter. Decoupled weight decay regularization. *arXiv preprint arXiv:1711.05101*, 2017.
- [25] OpenAI. GPT-4 technical report. *CoRR*, abs/2303.08774, 2023.
- [26] Maxime Oquab, Timothée Darcet, Théo Moutakanni, Huy Vo, Marc Szafraniec, Vasil Khalidov, Pierre Fernandez, Daniel Haziza, Francisco Massa, Alaaeldin El-Nouby, Mahmoud Assran, Nicolas Ballas, Wojciech Galuba, Russell Howes, Po-Yao Huang, Shang-Wen Li, Ishan Misra, Michael G. Rabbat, Vasu Sharma, Gabriel Synnaeve, Hu Xu, Hervé Jégou, Julien Mairal, Patrick Labatut, Armand Joulin, and Piotr Bojanowski. DINOv2: Learning robust visual features without supervision. *CoRR*, abs/2304.07193, 2023.
- [27] Xiaohuan Pei, Tao Huang, and Chang Xu. Efficientvmamba: Atrous selective scan for light weight visual mamba. *CoRR*, abs/2403.09977, 2024.
- [28] Alec Radford, Jong Wook Kim, Chris Hallacy, Aditya Ramesh, Gabriel Goh, Sandhini Agarwal, Girish Sastry, Amanda Askell, Pamela Mishkin, Jack Clark, Gretchen Krueger, and Ilya Sutskever. Learning transferable visual models from natural language supervision. In *ICML*, volume 139, pages 8748–8763. PMLR, 2021.
- [29] Ilija Radosavovic, Raj Prateek Kosaraju, Ross B. Girshick, Kaiming He, and Piotr Dollár. Designing network design spaces. In *CVPR*, pages 10425–10433. IEEE, 2020.
- [30] Karen Simonyan and Andrew Zisserman. Very deep convolutional networks for large-scale image recognition. In *ICLR*, 2015.
- [31] Mingxing Tan and Quoc V. Le. Efficientnet: Rethinking model scaling for convolutional neural networks. In *ICML*, volume 97, pages 6105–6114. PMLR, 2019.
- [32] Hugo Touvron, Matthieu Cord, Matthijs Douze, Francisco Massa, Alexandre Sablayrolles, and Hervé Jégou. Training data-efficient image transformers & distillation through attention. In *ICML*, volume 139, pages 10347–10357. PMLR, 2021.
- [33] Hugo Touvron, Matthieu Cord, and Hervé Jégou. DeiT III: revenge of the vit. In *ECCV*, volume 13684, pages 516–533. Springer, 2022.
- [34] Hugo Touvron, Thibaut Lavril, Gautier Izacard, Xavier Martinet, Marie-Anne Lachaux, Timothée Lacroix, Baptiste Rozière, Naman Goyal, Eric Hambro, Faisal Azhar, Aurélien Rodriguez, Armand Joulin, Edouard Grave, and Guillaume Lample. Llama: Open and efficient foundation language models. *CoRR*, abs/2302.13971, 2023.
- [35] Ashish Vaswani, Noam Shazeer, Niki Parmar, Jakob Uszkoreit, Llion Jones, Aidan N. Gomez, Lukasz Kaiser, and Illia Polosukhin. Attention is all you need. In *NeurIPS*, pages 5998–6008, 2017.
- [36] Tete Xiao, Yingcheng Liu, Bolei Zhou, Yuning Jiang, and Jian Sun. Unified perceptual parsing for scene understanding. In *ECCV*, pages 418–434, 2018.
- [37] Rui Xu, Shu Yang, Yihui Wang, Bo Du, and Hao Chen. A survey on vision mamba: Models, applications and challenges. *arXiv preprint arXiv:2404.18861*, 2024.
- [38] Chenhongyi Yang, Zehui Chen, Miguel Espinosa, Linus Ericsson, Zhenyu Wang, Jiaming Liu, and Elliot J. Crowley. Plainmamba: Improving non-hierarchical mamba in visual recognition. *CoRR*, abs/2403.17695, 2024.
- [39] Hanwei Zhang, Ying Zhu, Dan Wang, Lijun Zhang, Tianxiang Chen, and Zi Ye. A survey on visual mamba. *arXiv preprint arXiv:2404.15956*, 2024.
- [40] Xiaosong Zhang, Yunjie Tian, Lingxi Xie, Wei Huang, Qi Dai, Qixiang Ye, and Qi Tian. Hivit: A simpler and more efficient design of hierarchical vision transformer. In *ICLR*. OpenReview.net, 2023.
- [41] Lianghui Zhu, Bencheng Liao, Qian Zhang, Xinlong Wang, Wenyu Liu, and Xinggang Wang. Vision mamba: Efficient visual representation learning with bidirectional state space model. *CoRR*, abs/2401.09417, 2024.